Article ID: 1000-324X(2023)03-0322-07 **DOI:** 10.15541/jim20220353

High Quality and Large Size Yttrium Iron Garnet Crystal Grown by Top Seeded Solution Growth Technique

YANG Xiaoming[1], LAN Jianghe[2,3], WEI Zhantao[3], SU Rongbing[1], LI Yang[3], WANG Zujian[1], LIU Ying[1], HE Chao[1], LONG Xifa[1]

(1. Fujian Institute of Research on the Structure of Matter, Chinese Academy of Sciences, Fuzhou 350002, China; 2. School of Electronic Science and Engineering, University of Electronic Science and Technology of China, Chengdu 610054, China; 3. Southwest Institute of Applied Magnetics, Mianyang 621000, China)

Abstract: Yttrium iron garnet ($Y_3Fe_5O_{12}$, YIG) crystals have been widely used in microwave and magneto-optic devices due to their excellent magnetic and magneto-optical properties. Currently, the commercial material is YIG single crystal thin films, which is deposited on $Gd_3Ga_5O_{12}$ (GGG) substrate using liquid phase epitaxy technique. Herein, we report a new growth technology of YIG single crystal by top seeded solution growth (TSSG) technique from lead-free B_2O_3-BaF_2 flux. The maximum size and weight of the as-grown YIG crystal can be up to 43 mm× 46 mm×11 mm and 60 g, respectively. The crystals exhibit excellent comprehensive performances with narrow ferromagnetic resonance linewidth (0.679 Oe, 1 Oe=250/π A/m), high transparency (75%) and Faraday rotation angle (200 (°)·cm^{-1}@1310 nm and 160 (°)·cm^{-1}@1550 nm), indicating a good candidate in microwave and magneto-optic devices. More significantly, this growth technique is ideally suited to large size YIG or doped-YIG single crystals ascombined with the oriented seed crystal and lifting process, which can significantly decrease the manufacture cost.

Key words: yttrium iron garnet; single crystal; TSSG method; ferromagnetic resonance linewidth; magneto-optic effect

Recently, ultrahigh speed and large capacity information transmission system achieved much more attention with the development of the 5th generation communication techniques[1]. In practical application process, the optical data signal is inevitably distorted due to optical interference and filtering effects[2]. Therefore, the optical isolators[3] are needed to achieve unidirectional transport by preventing the reflected light into the laser sources[4]. Magneto-optic materials is the key material of this kind of nonreciprocal devices[5-8]. Among many magneto-optical materials, yttrium iron ferrimagnetic garnet crystals ($Y_3Fe_5O_{12}$, abbreviated as YIG) are important representative with suitable magnetic and electrical properties[9-10], that have been widely used as the key components in microwave communications and magneto-optical field due to their huge Faraday rotation angle[11] and excellent light transmission function in near and mid-infrared wavelength region[12-14].

So far, the commercial magneto-optic materials are mainly Bi and rare-earth doped YIG single crystal thin films, which is deposited on $Gd_3Ga_5O_{12}$ (GGG) substrate from the lead-based flux using a liquid phase epitaxy (LPE) technique[15-16] or pulsed laser deposition[17-18]. The films may contain some divalent and tetravalent Pb impurities that further affect the magnetic properties[19]. Moreover, the LPE method requires expensive GGG crystal substrates, and the maximum thickness of the film is only about 1 mm. YIG single crystal can also be grown by Floating Zone method[20] with the size up to 8 mm in diameter and 50 mm in length[14]. The fiber crystal has the advantages of good crystallinity and fast growth rate[21]. However, this growth technique is inappropriate for large-scale production due to high cost and low uniformity[22]. In this sense, it is of great significance to find a suitable method that can grow large size YIG crystal and realize large-scale productivity[23].

Top seeded solution growth (TSSG) technique has strong applicability for refractory, volatile and inconsistent melting system[24]. It has numerous advantages: (1) the growth process can be monitored in real time; (2) the

Received date: 2022-06-24; **Revised date:** 2022-08-14; **Published online:** 2022-10-25
Foundation item: National Natural Science Foundation of China (51902307, 11974349, 11904362, 52172009, 52102011)
Biography: YANG Xiaoming (1990–), male, associate professor. E-mail: xmyang@fjirsm.ac.cn
杨晓明(1990–), 男, 副研究员. E-mail: xmyang@fjirsm.ac.cn
Corresponding author: LAN Jianghe, senior engineer. E-mail: lanjh418915@sina.com; LONG Xifa, professor. E-mail: lxf@fjirsm.ac.cn
蓝江河, 高级工程师. E-mail: lanjh418915@sina.com; 龙西法, 研究员. E-mail: lxf@fjirsm.ac.cn

seed growth reduces the nucleation and benefit to obtain large size crystal; (3) the crystal has high uniformity[25]. Since 1958, Nielsen has begun to grow YIG single crystals from lead flux by molten salt method[26]. In the following decades, lead-based flux was the main flux due to their low melting point and high fluidity, such as PbO-PbF_2[27], PbF_2-B_2O_3[28], PbO-PbF_2-B_2O_3[29]. However, the crystal grown from the Pb-based flux contains some undesired impurities and intrinsic defects, which severely affect the microwave and magneto-optic properties[19]. Based on this, the lead-free flux began to attract the attention of researchers, such as BaO-B_2O_3[30], Na_2O-B_2O_3[31], BaO-BaF_2-B_2O_3[32]. In recent years, both the size and quality of YIG crystals have been improved gradually with the advent of the accelerated crucible rotation technique[33] and modified seeding procedure[34]. However, the preparation of large size and high quality YIG single crystal remains a huge and longstanding challenge.

In this work, the authors devoted to prepare large size YIG single crystals that could provide garnet crystals of satisfactory quality for commercial applications. The growth, crystal structure and basic properties of YIG single crystals prepared from the B_2O_3-BaF_2 flux were reported detailedly.

1 Experimental

The YIG crystals were grown by TSSG technique with B_2O_3-BaF_2 fluxes. Compared with lead-based flux, this lead-free flux has numerous advantages of nontoxicity, high solubility, low solvent incorporation and non-corrosion for platinum crucible[19]. The high purity starting chemicals (99.99%) of Y_2O_3, Fe_2O_3 and flux were weighed according to the stoichiometric composition of $Y_3Fe_5O_{12}$, and the optimal molar ratio of solute/flux. The weighed raw materials were thoroughly mixed in tumbling mixer and loaded into platinum crucible, then heated above the saturation temperature to 1200 ℃ for 48 h to ensure homogenization. A columnar [110]-orientated YIG crystal was used to determine the saturation temperature by repeated seeding trials and then grown at a rate of 0.2–0.5 ℃/h. After the growth process, the grown crystal was cooled down to room temperature at a rate of 30 ℃/h. Fig. 1 shows that the as-grown YIG crystals covered with the natural growth faces of (110) and (211) planes, which is mainly because the above-mentioned planes contain two and one easy directions of magnetization, respectively. After exploration and optimization of the growth process conditions, the size and weight of the single crystals were gradually increased, and the maximun size and weight of the as-grown YIG crystal can up to 43 mm×45 mm×11 mm and 60 g, respectively.

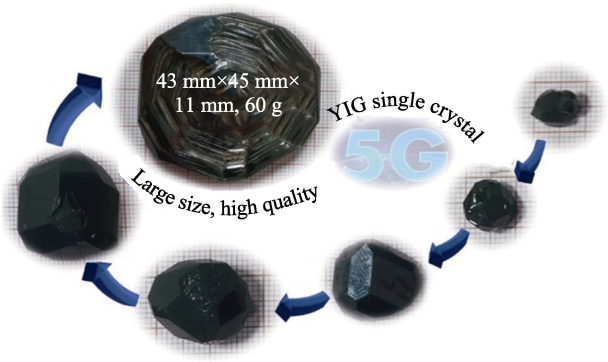

Fig. 1　Photo showing formation process of as-growth YIG single crystals

The X-ray diffraction (XRD) pattern was obtained by a diffractometer with Cu K_α radiation (Rigaku, Ultima IV, Japan). The structure data was collected on a single crystal X-ray diffractometer (Bruker D8, Mo K_α, λ= 0.071073 nm) at room temperature and the crystal structure was determined using the SHELXL software. The magnetic properties were measured by physical property measurement system (Quantum Design, model 6000, America). The dielectric properties were measured using an Alpha-broadband dielectric spectrometer (Novocontrol GmbH, Germany). The ferromagnetic resonance (FMR) data were obtained on the selected spheres at 5 GHz by a FMR tester. The crystal wafer was doubly-polished to optical grade with the thickness of 486 μm for transmission spectra scheme from 1000 nm to 2300 nm, which was measured by a UV-Vis-nearinfrared spectrophotometer (Perkin Elmer, Lamda 950, America). The X-ray photoelectron spectroscopy (XPS) characterization was performed by an XPS Spectrometer (Thermo Fisher, ESCALAB 250Xi, America).

2 Results and discussion

In the crystal growth process, $YFeO_3$ phase is easily incorporated with YIG crystal at the condition of high temperature[35]. Therefore, the high quality YIG seed crystal should be seeded to avoid the occurrence of $YFeO_3$ phase. Fig. 2(a) shows the XRD pattern of YIG crystal, exhibiting a pure garnet structure without any second phase in the apparatus resolution, which is accordance with the standard card (PDF#43-0507).

The garnet structure of YIG crystal was measured at room temperature, which is shown in Fig. 2(b). The crystal structure shows that YIG belongs to the cubic crystallographic system with a space group of Ia3d. The lattice parameters are a=b=c=1.23790 nm, α=β=γ=90° and Z=8, which is completely consistent with the previous data[36]. Fig. 2(c, d) show the sublattice structure and oxygen coordination around the Y^{3+} and Fe^{3+} ions in the

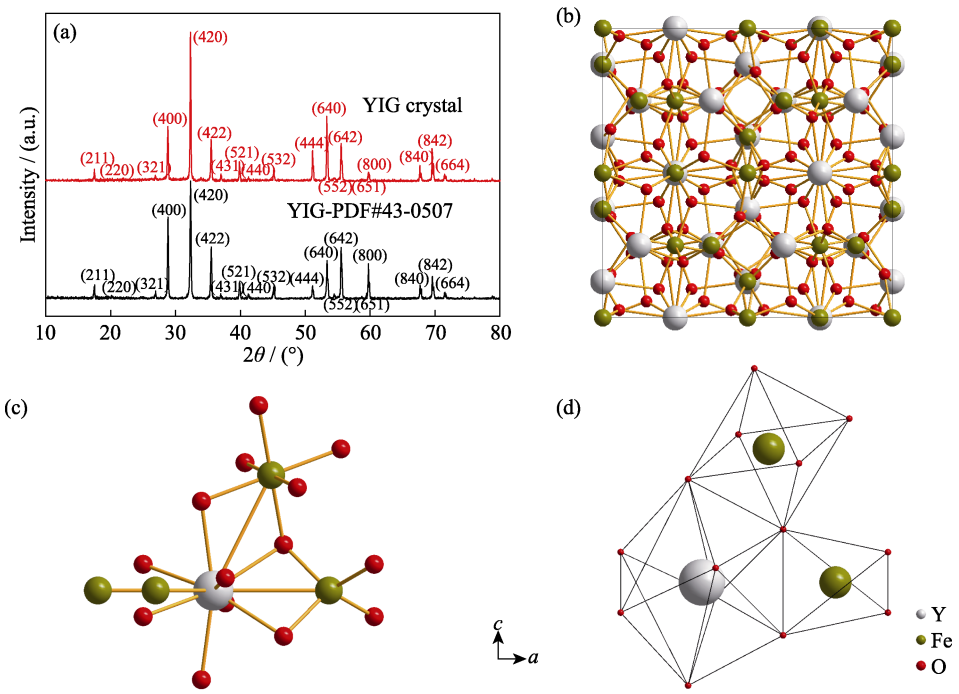

Fig. 2 XRD patterns and garnet structure of YIG crystal

(a) XRD patterns and standard diffraction card; (b) Garnet structure; (c) Positions and sublattice structure of positive ions; (d) Oxygen coordination of positive ions

lattice. Obviously, YIG crystal possesses three sublattices, *i.e.* Fe^{3+} ions occupied the octahedral A-sites and tetrahedral D-sites, and Y^{3+} ions occupied the dodecahedral C-sites[37]. The dodecahedral coordination Y^{3+} ions are diamagnetic and do not contribute to the optical or magnetic properties[38]. Nevertheless, Fe^{3+} ions at A-sites and D-sites sublattices surrounded by oxygen ions are separated, *i.e.* the spins of two Fe^{3+} ions at A-sites are antiparallel to that of three Fe^{3+} ions at D-sites, forming a net magnetization and Faraday rotation through the ferromagnetically coupled interaction[39-40]. The magnetic and magneto-optic properties of the as-grown YIG crystal are elaborated below.

For magnetic materials, the saturation magnetization (M_S), Curie temperature (T_C), dielectric constant (ε') and ferromagnetic resonance (FMR) linewidth are considered important indicators in the applications of linear and nonlinear microwave devices. Fig. 3(b) exhibits the magnetization-field (*M-H*) curve of YIG crystal at room temperature with the saturation magnetization of 25.43 emu/g (1 emu=10^{-3} A/m^2), showing a typical ferromagnetic characteristic. Fig. 3(a) shows the magnetic hysteresis loop in the magnetic field intensity of –1000–1000 Oe to facilitate the observation of hysteresis. The coercive field (H_c) of YIG crystal is 8.61 Oe, and the remnant magnetization (M_r) is 0.84 emu/g. It is concluded that the coercive field of YIG crystal is small enough, indicating that the saturation magnetization can be achieved only with a small external magnetic field, which significantly reducing the requirements for external magnetic field in magneto-optic applications. Fig. 3(c) depicts the temperature-dependent magnetization for an applied magnetic field of 1000 Oe for YIG crystal. The ferrimagnetic to paramagnetic transition temperature (T_C) was about 560 K, which is comparable to the previous reported data[38, 41].

Fig. 4(a, b) depicts the temperature-dependent dielectric constant (ε') and dielectric loss (tanδ) at various frequencies of 10 Hz–1 MHz. Obviously, the temperature-dependent ε' exhibits very high frequency stability below 100 ℃, and tanδ at 1 MHz is only about 8.9×10^{-4}. This is completely different from the $Lu_3Fe_5O_{12}$[42] and $Ho_3Fe_5O_{12}$[43] system, which exhibiting the typical relaxor behavior.

It is well known that the impurities and intrinsic defects severely affect the microwave losses[44]. Therefore, the quality of the YIG crystal with regard to microwave applications was measured using the FMR tester, which were obtained on the selected spheres at 5 GHz. The small YIG resonator spheres with the diamater of 0.5 mm are shown in Fig. 4(c). The FMR linewidth (ΔH) of the YIG spheres (signed by sample S1-S6) and the average ΔH are shown in Fig. 4(c, d). The values of ΔH reflect the presence of the fluctuations for the six sphere samples, which is mainly attribute to the sphericity or the crystal defects. As a result, the average ΔH is 0.679 Oe, which is comparable to the previous reported YIG crystal[45].

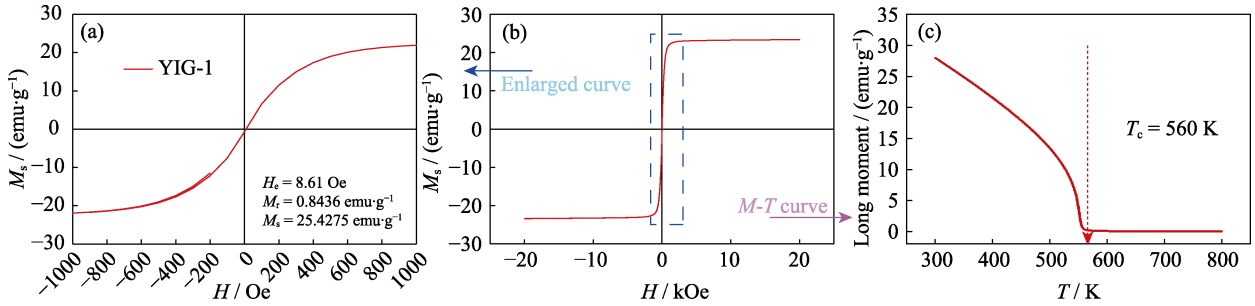

Fig. 3　Magnetic properties of YIG crystal

(a) Enlarged *M-H* curve in the magnetic field of –1000–1000 Oe; (b) *M-H* curve at room temperature;
(c) Temperature-dependent magnetization for an applied magnetic field of 1000 Oe (1 emu=10^{-3} A·m^{-2}, 1 Oe=250/π A·m^{-1})

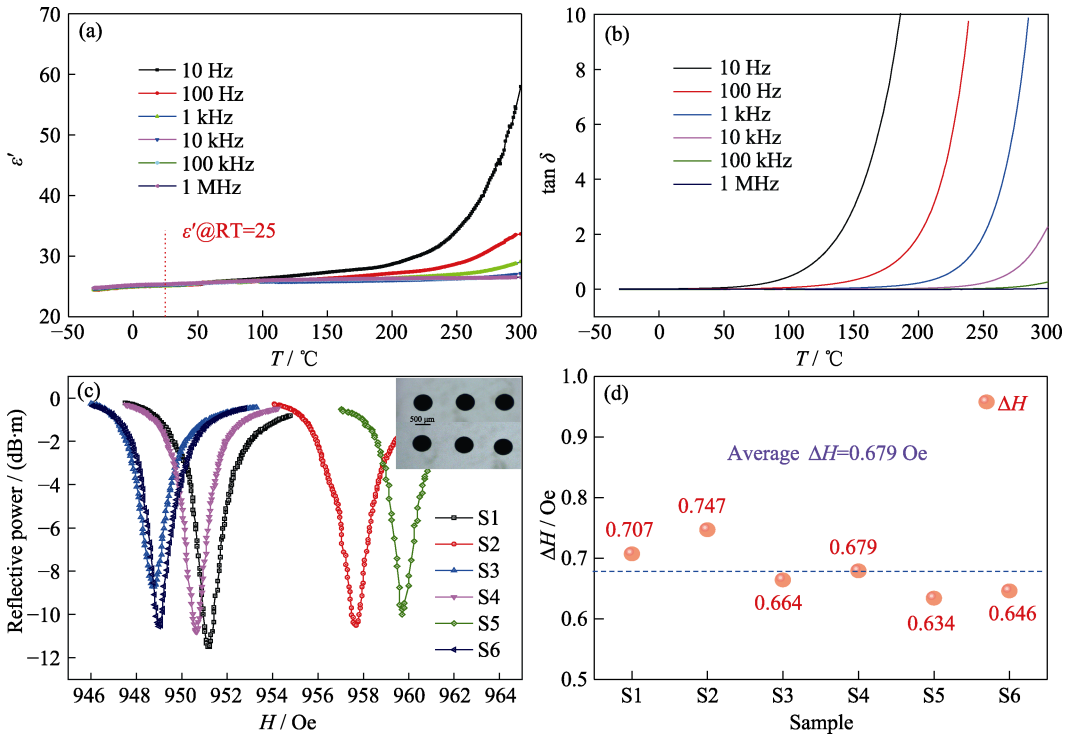

Fig. 4　Dielectric properties and FMR linewidth of YIG crystal

(a, b) Temperature dependent dielectric constant (ε′) and loss (tanδ) measured at the frequencies of 10 Hz–1 MHz;
(c) FMR linewidth of the YIG spheres showed in the upright inset; (d) Average Δ*H* of the spheres (1 Oe=250/π A·m^{-1})
Colorful figure is available on website

The YIG wafers were polished to optical grade with no anti-reflective coating for transmission spectrum measurement in the near infrared region of 980 to 2300 nm, which is shown in Fig. 5. Obviously, it possesses an intense absorption edge from 980 nm which influence extends out to about 1180 nm, and then the optical absorption becomes extremely lower in the wavelength of ~1180 nm. It was more significant that the transmittance at 1310 and 1550 nm are both higher than 75%, exhibiting a high level of transparency. According to the previous reports, the ideal transparency for pure YIG in the near infrared region is about 75%[46]. The results showed that the transmittance of the as-grown YIG crystal is very close to the theoretical value, which is consistent with the previously data.

In addition, the Faraday rotation angle of YIG crystal at the wavelength of 1310 and 1550 nm were 200 and 160 (°)·cm^{-1}, respectively, which is lower than the previously reported data (~220 (°)·cm^{-1}@1310 nm)[47-48].

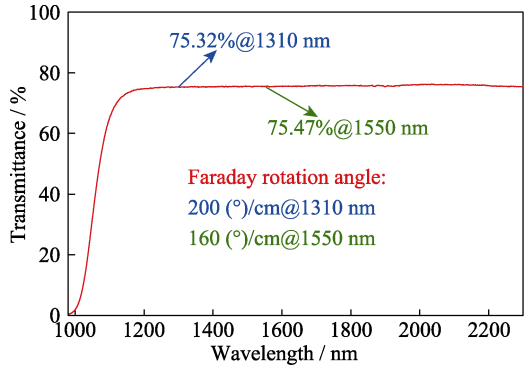

Fig. 5　Transmittance of YIG crystal and Faraday rotation angle at 1310 and 1550 nm

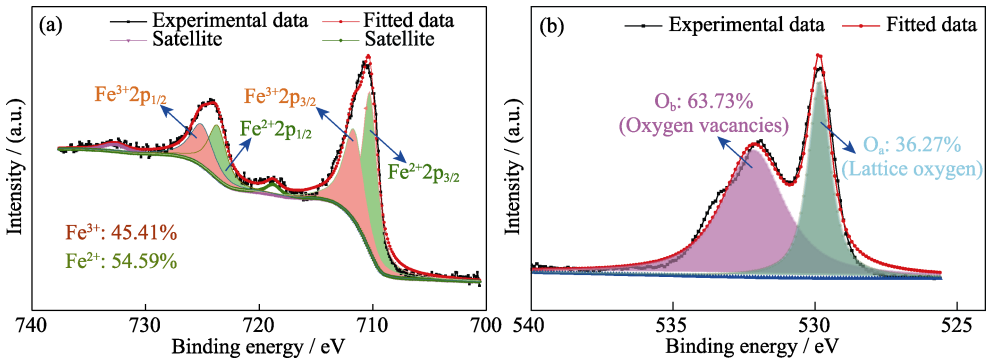

Fig. 6 X-ray photoelectron spectra and their Lorentzian-Gaussian dividing results of YIG crystal powders
(a) Fe2p; (b) O1s; Colorful figure is available on website

It is well known that the Faraday rotation effect is mainly attribute to the contribution of octahedral ferric ions[38]. However, the Fe^{3+} ions are easily reduced to Fe^{2+} ions in a low oxygen atmosphere[49] and the presence of Fe^{2+} ions will increase the optical absorption coefficient and weaken the Faraday rotation effect[50]. Therefore, we can speculate that the YIG crystal under the growth condition of a low oxygen partial pressure should contain large amounts of Fe^{2+} ions.

In order to identify the above speculation, the XPS technique was employed to check the valence of Fe and O element. Fig. 6 exhibits the X-ray photoelectron spectrum of Fe2p and O1s lines and their Lorentzian-Gaussian dividing results of YIG crystal powders. As shown in Fig. 6(a), the Fe2p core level splits into $2p_{1/2}$ and $2p_{3/2}$ components binding energy of around 724.6 and 710.9 eV, respectively. However, the peaks for Fe^{2+} and Fe^{3+} ions exhibit a mixed peak and can be fitted by the Lorentzian-Gaussian fitting method[51]. The fitting result show that the binding energy of $Fe2p_{1/2}$ is expected to be 725.23 eV for Fe^{3+} and 723.93 eV for Fe^{2+}, and the binding energy of $Fe2p_{3/2}$ is expected to be 711.73 eV for Fe^{3+} and 710.38 eV for Fe^{2+}[39]. Therefore, it is confirmed that the oxidation state of Fe ions in the as-grown YIG crystal are in a mixed Fe^{3+} and Fe^{2+} states[52]. The percentage of Fe^{2+} can be estimated by peak area according to the fitting curves, and the result shows that Fe^{2+} accounts for about 54.59% in octahedral A-sites and tetrahedral D-sites.

In addition, the valence fluctuation of Fe ions is always accompanied by the generation of oxygen vacancies. Fig. 6(b) shows the O1s spectrum of YIG crystal powders, which can be also splitted into two peaks. According to the fitting curves, the binding energy around 529.98 eV (O_a) represents the oxygen in the lattice, while the binding energy around 532.18 eV (O_b) is related to the oxygen vacancies. The percentage of oxygen vacancies can also be estimated by the integral area of the O_b peak, and the oxygen vacancies accounts for about 63.73%. The presence of Fe^{2+} valence state and oxygen vacancies must attribute to the low oxygen atmosphere at high-temperature growth process, which seriously increases the optical absorption coefficient and weaken the Faraday rotation effect. Therefore, the YIG crystal should be grown in oxygen atmosphere or nitrogen atmosphere in order to avoid generating the defects of Fe^{2+} and oxygen vacancies, and this will be a major focus in our future work.

3 Conclusions

Until now, there are many reports on the growth of YIG single crystals, but they are usually small in size and thickness. In this paper, we reported the growth optimization conditions for large-size YIG crystal by TSSG technique from lead-free B_2O_3-BaF_2 flux. The size and weight of the YIG crystal achieved 43 mm×46 mm×11 mm and 60 g with the natural growth faces of (110) and (211) planes. The crystals exhibited excellent purity, satisfactory quality and excellent comprehensive performances with the narrow ferromagnetic resonance linewidth (0.679 Oe), high transparency (75%) and Faraday rotation angle (200 (°)·cm^{-1}@1310 nm and 160 (°)·cm^{-1}@1550 nm), which makes it a promising candidate for microwave and magneto-optic device applications. XPS result shows that the as-grown YIG crystals possess some Fe^{2+} and oxygen vacancies, which must be originated from the low oxygen atmosphere in the high-temperature growth process, and this problem may be solved by introducing the oxygen atmosphere or nitrogen atmosphere.

References:

[1] AUNG Y L, IKESUE A, WATANABE T, *et al.* Bi substituted YIG ceramics isolator for optical communication. *Journal of Alloys and Compounds*, 2019, **811:** 152059.

[2] GUAN P, DA ROS F, LILLIEHOLM M, *et al.* Scalable WDM phase regeneration in a single phase-sensitive amplifier through optical time lenses. *Nature Communications*, 2018, **9:** 1049.

[3] KOBAYASHI N, IKEDA K, GU B, *et al.* Giant faraday rotation in metal-fluoride nanogranular films. *Scientific Reports*, 2018, **8:** 4978.

[4] GUDDALA S, KAWAGUCHI Y, KOMISSARENKO F, *et al.* All-optical nonreciprocity due to valley polarization pumping in transition metal dichalcogenides. *Nature Communications*, 2021, **12(1):** 3746.

[5] KOTOV V A, NUR-E-ALAM M, VASILIEV M, *et al*. Enhanced magneto-optic properties in sputtered Bi-containing ferrite garnet thin films fabricated using oxygen plasma treatment and metal oxide protective layers. *Materials*, 2020, **13(22):** 5113.

[6] LIN N X, LIN Y Z, WU G J, *et al.* Growth of high quality Si-based (Gd_2Ce) $(Fe_4Ga)O_{12}$ thin film and prospects as a magnetic recording media. *Journal of Alloys and Compounds*, 2021, **875:** 160086.

[7] WEI J W, HE H H. Computer aided design of magnetooptic properties for Bi-YIG film materials. *Journal of Inorganic Materials*, 1998, **13(2):** 251.

[8] ZOU S, HE X Y, ZENG X, *et al.* Microstructure and properties of Bi-doped yttrium iron garnet magneto-optical ceramics prepared by hot-pressing sintering process. *Journal of Inorganic Materials*, 2022, **37(7):** 773.

[9] NUR-E-ALAM M, VASILIEV M, BELOTELOV V, *et al.* Properties of ferrite garnet $(Bi, Lu, Y)_3(Fe, Ga)_5O_{12}$ thin film materials prepared by RF magnetron sputtering. *Nanomaterials*, 2018, **8(5):** 355.

[10] SORETO TEIXEIRA S, SALES A J M, GRATA M P F, *et al.* Yttrium ferrites with enhanced dielectric properties. *Materials Science and Engineering B*, 2018, **232:** 41.

[11] GOMI M, FURUYAMA H, ABE M. Strong magneto-optical enhancement in highly Ce-substituted iron garnet films prepared by sputtering. *Journal of Applied Physics*, 1991, **70(11):** 7065.

[12] MEI D J, CAO W Z, WANG N Z, *et al.* Breaking through the "3.0 eV wall" of energy band gap in mid-infrared nonlinear optical rare earth chalcogenides by charge-transfer engineering. *Materials Horizons*, 2021, **8(8):** 2330.

[13] KURIMOTO M, MATSUBAYASHI S, ANDO K, *et al.* Temperature dependence of the Faraday effect in Rh^{4+}-substituted magnetic garnets. *Journal of Applied Physics*, 1998, **83(9):** 4897.

[14] HIGUCHI S, FURUKAWA Y, TAKEKAWA S, *et al.* Magneto-optical properties of cerium-substituted yttrium iron garnet single crystals grown by traveling solvent floating zone method. *Japanese Journal of Applied Physics*, 1999, **38(7A):** 4122–4126.

[15] WANG H L, DU C H, Chris HAMMEL P, *et al.* Strain-tunable magnetocrystalline anisotropy in epitaxial $Y_3Fe_5O_{12}$ thin films. *Physical Review B*, 2014, **89(13):** 134404.

[16] FU J B, HUA M X, WEN X, *et al.* Epitaxial growth of $Y_3Fe_5O_{12}$ thin films with perpendicular magnetic anisotropy. *Applied Physics Letters*, 2017, **110(20):** 202403.

[17] KRYSZTOFIK A, OZOGLU S, MCMICHAEL R D, *et al.* Effect of strain-induced anisotropy on magnetization dynamics in $Y_3Fe_5O_{12}$ films recrystallized on a lattice-mismatched substrate. *Scientific Reports*, 2021, **11(1):** 14011.

[18] ZHANG Y, WANG C T, LIANG X, *et al.* Enhanced magneto-optical effect in $Y_{1.5}Ce_{1.5}Fe_5O_{12}$ thin films deposited on silicon by pulsed laser deposition. *Journal of Alloys and Compounds*, 2017, **703:** 591.

[19] KUCERA M, NITSCH K, STEPANKOVA H, *et al.* Growth and characterization of high purity epitaxial yttrium iron garnet films grown from BaO-B_2O_3-BaF_2 flux. *Physica Status Solidi A*, 2003, **198(2):** 407.

[20] HIGUCHI S, FURUKAWA Y, TAKEKAWA S, *et al.* Magnetooptical properties of cerium-substituted yttrium iron garnet single crystals for magnetic-field sensor. *Sensors and Actuators A-Physical*, 2003, **105(3):** 293.

[21] SEKIJIMA T, SATOH H, TAHARA K, *et al.* Growth of fibrous YIG single crystals by the self-adjusting solvent FZ method. *Journal of Crystal Growth*, 1998, **193(3):** 446.

[22] ISHIKAWA H, NAKAJIMA K, MACHIDA K, *et al.* Optical isolators using Bi-substituted rare-earth iron garnet films. *Optical and Quantum Electronics*, 1990, **22(6):** 517.

[23] IKESUE A, AUNG Y L, YASUHARA R, *et al.* Giant Faraday rotation in heavily Ce-doped YIG bulk ceramics. *Journal of the European Ceramic Society*, 2020, **40(15):** 6073.

[24] YE N, TU C Y, LONG X F, *et al.* Recent advances in crystal growth in china: laser, nonlinear optical, and ferroelectric crystals. *Crystal Growth & Design*, 2010, **10(11):** 4672.

[25] HE C, YANG X M, WANG Z J, *et al.* Relaxor-based ferroelectric single crystals grown by top-seeded solution growth method. *Scientia Sinica Technologica*, 2017, **47(11):** 1126.

[26] NIELSEN J W. Growth of magnetic garnet crystals. *Journal of Applied Physics*, 1958, **29(3):** 390.

[27] NIELSEN J W. Improved method for the growth of yttrium-iron and yttrium-gallium garnets. *Journal of Applied Physics*, 1960, **31(5):** S51.

[28] ANTONINI B, PAOLETTI A, PAROLI P. Isothermal growth of bulk YIG crystals by PbF_2-B_2O_3 flux evaporation. *Journal of Crystal Growth*, 1981, **54(3):** 586.

[29] TOLKSDORF W. Growth of magnetic garnet single crystals from high temperature solution. *Journal of Crystal Growth*, 1977, **42:** 275.

[30] LINARES R C. Growth of yttrium-iron garnet from molten barium borate. *Journal of the American Ceramic Society*, 1962, **45(7):** 307.

[31] BANDYOPADHYAY T, SAHA P. Growth of yttrium iron garnet single crystals in Na_2O-B_2O_3 flux system in air. *Pramana*, 1977, **9(2):** 111.

[32] NIKOLOV V, ILIEV K, PESHEV P. Stability region and growth conditions of Al-and Ga-substituted $Y_3Fe_5O_{12}$ single crystals in solvents from the BaO-B_2O_3-BaF_2 system. *Materials Research Bulletin*, 1982, **17(1):** 47.

[33] WENDE G, GORNERT P. Study of ACRT influence on crystal growth in high-temperature solutions by the "high-resolution induced striation method". *Physica Status Solidi A*, 1977, **41(1):** 263.

[34] NIKOLOV V, ILIEV K, PESHEV P. Effect of the hydrodynamics in high-temperature solutions on the quality of pure and substituted YIG single crystals grown by the TSSG method. *Journal of Crystal Growth*, 1986, **75(2):** 269.

[35] OKA K, UNOKI H. $Y_3Fe_5O_{12}$ single-crystal growth by top seeded solution growth method. *Journal of Applied Physics*, 1984, **56(2):** 436.

[36] GUO X F, TAVAKOLI A H, SUTTON S, *et al.* Cerium substitution in yttrium iron garnet: valence state, structure, and energetics. *Chemistry of Materials*, 2014, **26(2):** 1133.

[37] GILLEO M A, GELLER S. Magnetic and crystallographic properties of substituted yttrium-iron garnet, $3Y_2O_3$-xM_2O_3-$(5–x)$ Fe_2O_3. *Physical Review*, 1958, **110(1):** 73.

[38] ENOCH R D. Magnetic domain studies on yttrium iron garnet using an infrared image converter. *Contemporary Physics*, 1975, **16(6):** 561.

[39] WU H R, HUANG F Z, XU T T, *et al.* Magnetic and magnetodielectric properties of $Y_{3-x}La_xFe_5O_{12}$ ceramics. *Journal of Applied Physics*, 2015, **117(14):** 144101.

[40] LI H Y. Investigation of the structural, magnetic, impedance properties in samarium-doped yttrium iron garnet. *Ceramics International*, 2020, **46(10):** 15408.

[41] AAKANSHA, DEKA B, RAVI S. Magnetic and dielectric properties of $Y_{3-x}Sm_xFe_5O_{12}$ (x=0 to 3.0). *Journal of Superconductivity and Novel Magnetism*, 2018, **31(7):** 2121.

[42] WU X B, WANG X F, LIU Y F, *et al.* Study on dielectric and magnetodielectric properties of $Lu_3Fe_5O_{12}$ ceramics. *Applied Physics*

Letters, 2009, **95(18):** 182903.
[43] SU J, LU X M, ZHANG C, *et al.* The effect of sintering temperature on magnetic and dielectric properties of $Ho_3Fe_5O_{12}$ ceramics. *Journal of Materials Science*, 2011, **46(10):** 3488.
[44] KUCERA M, NITSCH K, MARYSKO M, *et al.* Properties of epitaxial yttrium iron garnet films grown from BaO flux. *Journal of Applied Physics*, 2003, **93(10):** 7510.
[45] STRIATIONS I, GORNERT P, HERGT R. Preparation and crystal imperfections of yttrium-iron garnet single crystals grown in flux melts by slowly cooling and gradient transport I. Striations. *Physica Status Solidi A*, 1973, **20(2):** 577.
[46] FURUKAWA Y, FUJIYOSHI M, NITANDA F, *et al.* Valency control of iron in $Y_3Fe_5O_{12}$ single crystals grown by the floating zone method. *Journal of Crystal Growth*, 1994, **143(3/4):** 243.
[47] MATSUMOTO S, SUZUKI S. Temperature-stable Faraday rotator material and its use in high-performance optical isolators. *Applied Optics*, 1986, **25(12):** 1940.
[48] ISHIKAWA H, NAKAJIMA K, MACHIDA K, *et al.* Optical isolators using Bi-substituted rare-earth iron garnet films. *Optical and Quantum Electronics*, 1990, **22(6):** 517.
[49] SEKIJIMA T, ITOH H, FUJII T, *et al.* Influence of growth atmosphere on solubility limit of Ce^{3+} ions in Ce-substituted fibrous yttrium iron garnet single crystals. *Journal of Crystal Growth*, 2001, **229(1):** 409.
[50] ANTONINI B, BLANK S L, LAGOMARSINO S, *et al.* Oxidizing effects of high temperature annealing in reducing atmosphere in Ca-doped YIG films. *Journal of Magnetism and Magnetic Materials*, 1980, **20(2):** 216.
[51] SHANNIGRAHI S R, HUANG A, CHANDRASEKHAR N, *et al.* Sc modified multiferroic $BiFeO_3$ thin films prepared through a sol-gel process. *Applied Physics Letters*, 2007, **90(2):** 022901.
[52] LARSEN P K, METSELAA.R. Electric and dielectric properties of polycrystalline yttrium iron garnet: space-charge-limited currents in an inhomogeneous solid. *Physical Review B*, 1973, **8(5):** 2016.

顶部籽晶法生长大尺寸、高品质钇铁石榴石晶体

杨晓明[1], 蓝江河[2,3], 魏占涛[3], 苏榕冰[1], 李 阳[3],
王祖建[1], 刘 颖[1], 何 超[1], 龙西法[1]

(1. 中国科学院 福建物质结构研究所, 福州 350002; 2. 电子科技大学 电子科学与工程学院, 成都 610054; 3. 西南应用磁学研究所, 绵阳 621000)

摘 要: 钇铁石榴石($Y_3Fe_5O_{12}$, YIG)晶体具有优异的磁学和磁光性质, 在微波和磁光器件中有着广泛的应用。目前商用的磁光材料是采用液相外延技术在 $Gd_3Ga_5O_{12}$(GGG)衬底上沉积的 YIG 单晶薄膜。本研究以无铅 B_2O_3-BaF_2 为复合助熔剂, 采用顶部籽晶法技术(TSSG)生长 YIG 单晶材料, YIG 晶体尺寸和重量分别可达 43 mm×46 mm×11 mm 和 60 g。该晶体具有较窄的铁磁共振线宽(0.679 Oe)、高透明度(75%)和法拉第旋转角(200 (°)·cm^{-1}@1310 nm, 160 (°)·cm^{-1}@1550 nm)等优异的综合性能, 是微波和磁光器件的良好候选材料。更为重要的是, 这种生长技术非常适合大尺寸 YIG 单晶或稀土掺杂 YIG 单晶, 结合定向籽晶生长和提升工艺, 可以显著降低生产成本。

关 键 词: 钇铁石榴石; 单晶; 顶部籽晶法; 铁磁共振线宽; 磁光效应

中图分类号: TQ174 **文献标志码:** A